공학석사 학위논문

Study on Electron Cyclotron Heating (ECH) Pre-ionization in Versatile Experiment Spherical Torus (VEST)

VEST에서 전자 사이클로트론 가열을 이용한 전이온화에 대한 연구

2013년 8월

서울대학교 대학원

에너지시스템공학부

조 중 갑

Study on Electron Cyclotron Heating (ECH) Pre-ionization in Versatile Experiment Spherical Torus (VEST)

지도교수 황 용 석

이 논문을 공학석사 학위논문으로 제출함
2013년 08월

서울대학교 대학원
에너지시스템공학부
조 종 갑

조종갑의 공학석사 학위논문을 인준함
2013년 08월

위 원 장 나 용 수 (인)

부위원장 황 용 석 (인)

위 원 김 선 호 (인)

Abstract

Study on Electron Cyclotron Heating (ECH) Pre-ionization in Versatile Experiment Spherical Torus (VEST)

Jo, JongGab
Department of Energy System Engineering
The Graduate School
Seoul National University

Pre-ionization means the plasma production before ohmic discharge in tokamak to reduce the required loop voltage and to save the magnetic flux consumption for reliable start-up. ECH has been routinely used for pre-ionization in most tokamak devices, but in ST devices which have characteristics of high beta operation and low cutoff density, alternative method using the Electron Bernstein Wave (EBW) has been studied. In previous works, the effect of the profile of electron density and temperature on ECH pre-ionization has rarely researched. In this thesis, characteristics of

ECH pre-ionization in VEST device are investigated by measurement of the radial profile of electron density and temperature.

To analyze the tunneling and mode conversion of X-wave, two inhomogeneous cold plasma models are introduced. Especially, Budden analysis is applied in this study to interpret the experimental results of LFS X-mode injection.

ECH launching system of VEST has been designed to use low field side injection configuration based on the preliminary experimental result in linear device. Magnetron which can generate the frequency of 2.45GHz and maximum power of 6kW is installed. The triple probe is fabricated to diagnose the time varying plasma during discharges. Design requirements for the triple probe are determined by the electron density and temperature of target plasma estimated from the result of preliminary experiment. To confirm the validity of the triple probe data, the electron density is compared with interferometer.

The radial profile of electron density and temperature are measured using the triple probe for the ECH plasma in pre-ionization phase when only the toroidal magnetic field is applied and no loop voltage are provided. The ECH power, TF current and wave polarization are varied to examine the effect of each operating parameter on pre-ionization and to find the optimal pre-ionization condition. As the injected ECH power increases, it is observed that distance between the ECR and UHR is increased and high electron density is measured in front of the outer wall. As the TF strength decrease, the radial profile of electron density moves inboard side along the resonance layer and

maximum electron density is decreased by about 30%. However, when the plasma is produced near the inner wall with the lowest TF strength, high electron density comparable to that of the highest TF strength is measured. The second harmonic heating by FLR effect is observed but only when the pre-heated plasma exists and sufficient ECH power is transferred to the plasma. It is observed that the heating efficiency of the second harmonic heating is lower than that of the fundamental cyclotron heating. The result of O-mode injection is similar to that of X-mode injection, but the electron density is a little lower. The reflected microwave measured by rf power meter shows that the polarization of O-wave is converted into X-mode in the chamber.

Tunneling and mode conversion phenomena of X-wave in VEST are well described by Budden analysis. The reflection coefficients calculated from the experimental data show a good agreement with measured reflected microwave power during discharge. The mode conversion coefficient is calculated to be about 20% in VEST pre-ionization plasma. The LFS X-wave injection with direct X-B mode conversion can be possible as an effective method for pre-ionization in VEST. The effect of density scale length, magnetic field and chamber wall on tunneling and mode conversion is discussed to utilize the EBW for pre-ionization.

In VEST pre-ionization experiment, high density plasma is produced with the aid of high X-B mode conversion efficiency when the peak of density profile is near the inner wall or outer wall. However, high density plasma produced near the center region without loss of the TF strength is favorable to

start-up. For effective pre-ionization, two schemes can be suggested. First, the magnetic field structure during start-up can be utilized to increase the mode conversion efficiency in center region. During the start-up, high density plasma, which is confined in the magnetic field structure, can make the steep density gradient and L-cutoff layer located in center region increasing the mode conversion efficiency. Secondly, assistance of the second harmonic heating in the pre-heated plasma by adding another frequency source can be utilized. Although the heating efficiency of second harmonic heating is lower than fundamental heating in pre-ionization phase, the second harmonic EC wave doesn't encounter cutoff layer before reaching the 2^{nd} harmonic ECR without mode conversion. If the pre-heated plasma exists and sufficient ECH power is injected, the second harmonic heating can be used for central heating with high magnetic field operation.

The characteristic of ECH pre-ionization is investigated with the profile of electron density and temperature to find the effective pre-ionization condition. Also, the effective pre-ionization schemes are suggested based on the experimental results and analysis. This research is expected to contribute to the start-up and EBW study in VEST.

Keyword: Pre-ionization, ST, Electron Cyclotron Heating, VEST, Budden model, Tunneling, Mode conversion, Electron Bernstein Wave, Electron Cyclotron Resonance, Upper Hybrid Resonance

Student Number: 2011-21112

Contents

List of Tables

List of Figures

Chapter 1

Introduction

1.1 Motivation and objectives

Pre-ionization means the plasma production before ohmic discharge in tokamak to reduce the required loop voltage for breakdown and save the magnetic flux consumption. Especially pre-ionization is essential for Spherical Torus (ST) which has difficulty in start-up due to lack of space for the center stack. Many pre-ionization methods are utilized for the successful start-up such as Electron Cyclotron Heating (ECH), Ion Cyclotron Resonance Heating (ICRH) [1] and DC helicity injection [2], but ECH is most widely used method for pre-ionization because of many advantages as follows.

- Easy to launch wave far from the plasma
- Effective method for heating and current drive
- Well developed technology and theory
- Various applications like current profile and instability control

In previous works, issue of pre-ionization and start-up using ECH can be categorized by machine whether device is the conventional tokamak or ST. Cutoff frequency and density of EC wave is mainly determined by the

toroidal magnetic field. O-mode cutoff density is given by

$$n_c = \frac{B_t^2}{10.3} \times 10^{20} m^{-3} \tag{1.1}$$

In conventional tokamak, O1 mode or X2 mode is mainly used due to very high toroidal magnetic field and cutoff density. Table 1.1 shows the summarized information of wave polarization in various devices. Especially heating by high harmonic frequency of X-mode and related phenomenon such as the power threshold and delayed breakdown time has been studied.

Wave Polarization	**Device**	**Ref.**
O1	ITER, JT-60U	[3, 4]
X2	KSTAR, DIII-D	[5, 6]
X3	TCV	[7]

Table 1.1 Polarization of the launched wave in conventional tokamaks

In ST devices which have characteristics of high beta operation and low cutoff density, alternative method using the Electron Bernstein Wave (EBW) has been studied. The EBW is an electrostatic wave which has no cutoff density, but it can't be launched from outside of the plasma. Mode conversion schemes that convert electromagnetic waves into electrostatic waves are needed for exciting the EBW. According to the injected wave from the outside, mode conversion schemes are categorized into O-X-B and X-B. Table 1.2 shows the mode conversion scheme of ST devices.

Production of the overdense plasma using the EBW heating has been reported.

Mode Conversion Scheme	Device	Ref.
O-X-B	MAST, LATE	[8, 9]
X-B	NSTX, TST-2	[10, 11]

Table 1.2 EBW mode conversion schemes of ST devices

Obviously pre-ionization condition has a major effect on start-up in many researches. ECH pre-ionization is believed to be critical factor for successful start-up as explained in empirical Lloyd condition [12]. Pre-ionization reduces the required loop voltage and connection length for reliable start-up. However, although the importance of ECH pre-ionization is recognized and the ECH pre-ionization has been routinely used for the start-up in most tokamak devices, the underlying physics of the pre-ionization has not been revealed and the study on the pre-ionization itself has been started recently. Therefore, further research on ECH pre-ionization is essential for the understanding ECH assisted start-up and its effective application to tokamak device.

Furthermore, most of previous works have focused on the correlation between average electron density and plasma current generated in ohmic discharge phase. However, as ECH is a local heating method, pre-ionization condition can’t be discussed without the profiles of electron density and temperature. Propagation, absorption and reflection of EC wave

are significantly associated with profile of the plasma parameters. Thus, ECH mechanism with respect to the profile of plasma parameters is important for the understanding the pre-ionization. Also, it is obvious that higher electron density in pre-ionization phase has an advantage in start-up. Therefore, for effective pre-ionization, efficient plasma production with low ECH power is needed.

1.2 Preliminary experiment in linear device

A preliminary experiment was conducted in simple linear device which produce the ECR plasma in toroidal magnetic field by tilted magnet to determine the optimal wave launching configuration for pre-ionization in VEST as well as to find out possible EBW mode conversion scheme in VEST. Figure 1.1 is a picture of the linear device which consists of the quartz cylinder chamber and magnet. Microwave can be injected from low filed side or high field side through waveguide from magnetron launcher. Twisted waveguide is used to convert wave polarization of X-mode into O-mode. Driving frequency of 2.45GHz has been used with toroidal magnetic field of 875G at center and working gas of hydrogen same as VEST. To find the optimal condition for pre-ionization, electron density is measured with Langmuir probe with respect to injection direction and polarization of wave as shown in Figure 1.2. When microwave is injected from low field side, electron density is higher than that of high field side injection and X-mode is more favorable than O-mode for pre-ionization. Also, overdense plasma

exceeding the L-cutoff density has been observed which is probably produced by X-B mode conversion. The results of preliminary experiment show that X-mode injection from low filed side is the best condition for pre-ionization. ECH wave launching system of VEST is installed with LFS X-mode configuration based on results of preliminary experiment.

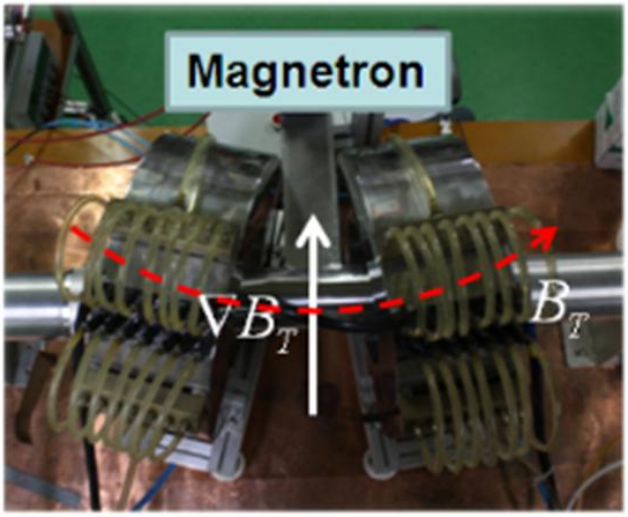

Figure 1.1 Picture of the linear device

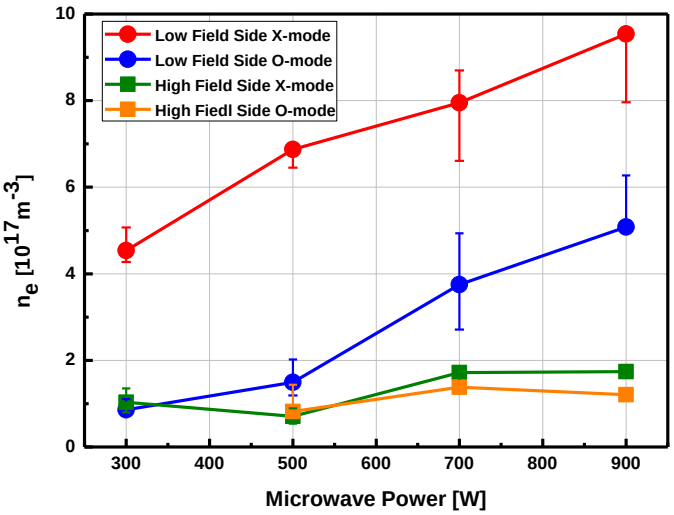

Figure 1.2 Electron density with respect to the microwave power, wave polarization and launching direction

1.3 Thesis outline

In this thesis, characteristics of ECH pre-ionization in VEST device are investigated by measurement of the radial profile of electron density and temperature during discharge and the experimental results are analyzed using inhomogeneous cold plasma model including tunneling, reflection and conversion of wave. The effective pre-ionization schemes are suggested based on the experimental results and analysis.

In chapter 2, theoretical backgrounds including cold plasma dispersion relation, inhomogeneous cold plasma models and finite Larmor radius effect are presented.

In chapter 3, ECH system in VEST and diagnostics for experiment are introduced. The triple probe theory is introduced and measured electron density is compared with interferometer to confirm the validity of the triple probe data.

In chapter 4, the results of ECH pre-ionization experiment are discussed. Characteristics of ECH plasma in pre-ionization phase with respect to operation parameters such as ECH power, TF strength and wave polarization are analyzed through Budden model.

In chapter 5, the results of this study are summarized and conclusions and future works are presented.

Chapter 2

Theoretical Background

2.1 Dispersion relation of cold plasma

2.1.1 Cold plasma dispersion relation

From the equation of motion and Maxwell equation, cold plasma dispersion relation can be derived for non trivial solution. It is assumed that plasma is homogeneous, particles have no kinetic thermal motion and the ion's motion is neglected. Dispersion relation of cold plasma can be expressed by Stix notation and following equations [13, 14]

$$An^4 - Bn^2 + C = 0 \tag{2.1}$$

where $A = S\sin^2\theta + P\cos^2\theta$, $B = RL\sin^2\theta + PS(1+\cos^2\theta)$ and $C = PRL$ or in terms of the angle

$$\tan^2\theta + \frac{P(n^2 - R)(n^2 - L)}{(Sn^2 - RL)(n^2 - P)} = 0 \tag{2.2}$$

General resonance and cutoff condition can be derived from the cold plasma dispersion relation. Resonance condition, where n goes to infinity, is given by

$$\tan^2\theta = -P/S \tag{2.3}$$

Cutoff condition, where n goes to zero, is given by

$$C = PRL = 0 \tag{2.4}$$

2.1.2 X-mode and O-mode

X-wave and O-wave is two branch of propagating wave perpendicular to magnetic field. For perpendicular propagation, equation (2.2) gives two dispersion relations for X-mode and O-mode.

$$n_X^2 = \frac{RL}{S} \tag{2.5}$$

$$n_O^2 = P \tag{2,6}$$

Table 2.1 shows the summarized resonance and cutoff condition of X-mode and O-mode. O-mode has no resonance in cold plasma dispersion relation and reflected at plasma frequency. X-mode has upper hybrid resonance and two cutoffs. O-mode is only affected by the plasma density but X-mode is affected by both plasma density and the magnetic field. It is caused by the polarization of wave. Electric field component of O-mode and X-mode is parallel and perpendicular to external magnetic field. Electric field parallel to the magnetic field has no interaction with magnetic field. Thus, X-wave is more complicated by effect of both the magnetic field and plasma. That's why the name is so called ordinary wave and extraordinary wave.

Wave polarization	**Resonance**	**Cutoff**
X-mode	S=0 (UHR)	R=0 (R-cutoff), L=0 (L-cutoff)
O-mode	No resonance	P=0 (plasma frequency)

Table 2.1 Resonance and cutoff condition of X-mode and O-mode

Various frequencies of cutoff and resonance are presented as follows

$$\omega_{pe} = \sqrt{\frac{n_e e^2}{m_e \varepsilon_0}} \tag{2,7}$$

$$\omega_{ce} = \frac{Bq}{m_e} \tag{2,8}$$

$$\omega_{UH} = \sqrt{\omega_{pe}^2 + \omega_{ce}^2} \tag{2,9}$$

$$\omega_R = \frac{1}{2}(\omega_{ce} + \sqrt{\omega_{ce}^2 + 4\omega_{pe}^2}) \tag{2,10}$$

$$\omega_L = \frac{1}{2}(-\omega_{ce} + \sqrt{\omega_{ce}^2 + 4\omega_{pe}^2}) \tag{2,11}$$

O-mode has no correlation with injected direction and magnetic field because of cutoff is determined only by the plasma density as mentioned above. Situations are more complicated for X-mode. Figure 2.1 shows the schematic diagram of X-wave launched from low field side. X-wave first encounters R-cutoff before reaching the UHR. In homogeneous plasma model, wave must be totally reflected at cutoff layer. However, if there are large gradient of the plasma density or magnetic field as in tokamak, inhomogeneous plasma model is needed for realistic description of wave.

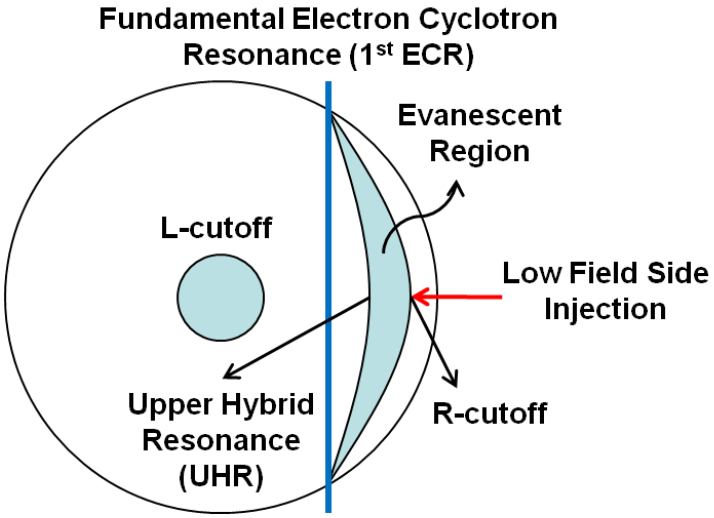

Figure 2.1 Schematic diagram of X-wave launched from low field side in tokamak

2.2 Inhomogeneous cold plasma model

Homogeneous plasma model couldn't explain the details of propagation and absorption near the resonance or cutoff region. If the change of plasma parameters and magnetic field is large over a wavelength, inhomogeneous plasma model must be applied for describing the behavior of the wave. Inhomogeneous plasma makes it possible to cross the boundaries in CMA diagram which means the resonance and cutoff. The tunneling and mode conversion of wave can occur at cutoff and resonance layer. Two models for solving the wave equation in resonance-cutoff pair region are introduced in sec 2.2.1 and 2.2.2.

2.2.1 Resonance-cutoff doublet (Budden problem)

In 1955, Budden [15] analyzed the tunneling effect in resonance-cutoff pair region. Budden set the wave number k as fractional function to solve the wave equation. Figure 2.2 shows the spatial variation of k(x) in Budden model. x=0 equal to UHR and R-cutoff is positioned at x=a. In his treatment, general resonance and cutoff can be substituted for upper hybrid resonance and R-cutoff to study the X-wave in tokamak. Wave equation is now given by

$$\frac{d^2E}{dx^2} + k^2(x)E = 0 \tag{2.12}$$

where $k^2(x) = k_0^2\left(1 - \frac{a}{x}\right)$. This equation can be solved analytically in Whittaker function [16]. Transmission, reflection and conversion coefficient can be evaluated through investigating the asymptotic form of solutions. Coefficients are expressed in terms of Budden parameter that has physical meaning of the distance between resonance and cutoff. Coefficients are given by [14]

$$T = e^{-2\eta} \tag{2.13}$$

$$R = (1 - e^{-2\eta})^2 \tag{2.14}$$

$$C = 1 - T - R = e^{-2\eta}(1 - e^{-2\eta}) \tag{2.15}$$

where Budden parameter $\eta = \frac{\pi k_0 a}{2}$. Transmission coefficient (T) means the fraction of X-wave propagating beyond the R-cutoff and reflection coefficient (R) means the fraction of X-wave reflecting at the R-cutoff. Conversion coefficient (C) is evaluated from the energy conservation law. The rest of the wave except the incoming and outgoing X-wave is the EBW excited by mode conversion in the UHR. Thus, conversion coefficient means the X-B mode conversion efficiency.

If thickness of the evanescent region is sufficiently smaller than wavelength, the incident wave can propagate beyond the cutoff and reach to the resonance layer. Figure 2.3 shows the change of coefficients with Budden parameter. Maximum value of conversion coefficient is 0.25 in optimum Budden parameter.

2.2.2 Cutoff-resonance-cutoff triplet

As explained in section 2.1.2, X-mode has two cutoffs of R-cutoff and L-cutoff. When high density L-cutoff layer is positioned near the UHR and R-cutoff, triplet model is needed to analyze the behavior of X-wave. Figure 2.4 shows the spatial variation of k(x) in triplet model. Analytic solution can't be available in this problem. Numerical schemes are needed to

obtain coefficients. Budden parameter is now expressed by [17]

$$\eta = \frac{\Omega_{ce} L_{ne}}{c} \frac{\kappa}{\sqrt{\kappa^2 + 2(L_{ne}/L_B)}} \left[\frac{\sqrt{1+\kappa^2} - 1}{\kappa^2 + (L_{ne}/L_B)\sqrt{1+\kappa^2}} \right]^{\frac{1}{2}} \qquad (2.16)$$

where L_{ne} and L_B are scale length of the electron density and magnetic field in the UHR and $\kappa = \left| \frac{\omega_{pe}}{\Omega_{ce}} \right|_{UHR}$. Maximum mode conversion coefficient is given by

$$C_{\max} = 4e^{-\pi\eta}(1 - e^{-\pi\eta}) \qquad (2.17)$$

Figure 2.5 shows the maximum conversion coefficient with respect to Budden parameter. From the calculated conversion coefficient, 100% mode conversion is possible theoretically. L-cutoff increases the conversion efficiency and can make maximum conversion coefficients of 1 with optimum condition for phase of incident wave and reflected wave.

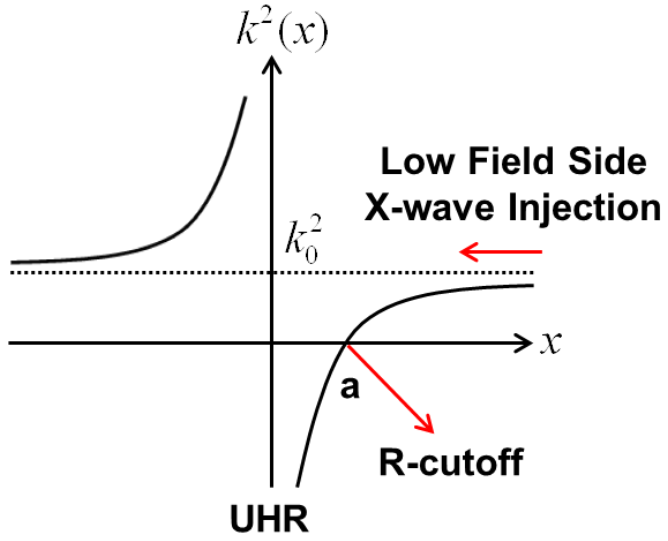

Figure 2.2 Spatial variation of k(x) in Budden model

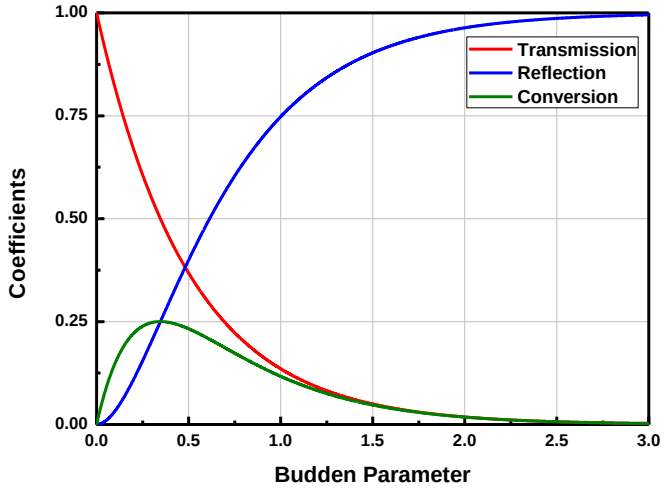

Figure 2.3 The change of transmission, reflection and conversion coefficient with Budden parameter

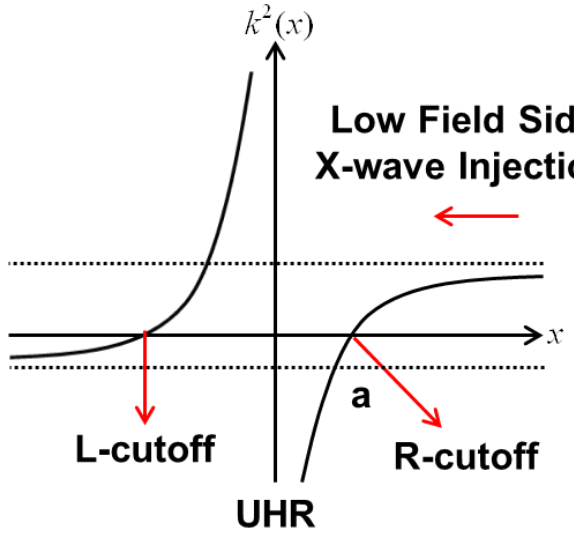

Figure 2.4 Spatial variation of k(x) in cutoff-resonance-cutoff triplet model

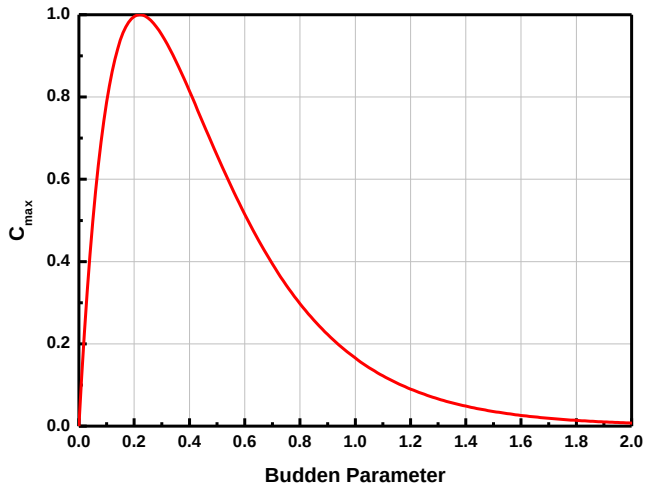

Figure 2.5 Maximum mode conversion coefficient with respect to Budden parameter

2.3 Finite Larmor Radius (FLR) effect

In cold plasma model, Larmor radius of charged particles is zero by putting the temperature equal to zero. However, when finite electron temperature is considered, influence of the magnetic field on the hot plasma introduces higher cyclotron harmonic effect which doesn't appear in cold plasma dispersion relation. [14] Finite Larmor Radius (FLR) dispersion relation is good approximation to the full hot plasma dispersion relation within the limit of $k_\perp \rho_e << 1$. For perpendicular propagation of X-wave, FLR dispersion relation can be written as [18].

$$\sigma n_\perp^4 - S n_\perp^2 + RL = 0 \tag{2.18}$$

where $\sigma \approx 3\frac{\omega_{pe}^2}{\omega^2}\frac{\omega^2\Omega_{ce}^2}{(\omega^2-\Omega_{ce}^2)(\omega^2-4\Omega_{ce}^2)}\frac{kT_e}{c^2 m_e}$ and R, L, S are Stix notation introduced in section 2.1. A new term σ is added in the equation (2.5) and $T_e = 0$ gives cold plasma dispersion relation again. The damping condition of wave can be estimated by investigating the discriminant of equation (2.18),

$$D = S^2 - 4\sigma RL < 0 \tag{2.19}$$

To satisfy the equation (2.19), σ must be nonzero with finite electron

temperature and it is shown that strong damping occur near the fundamental ECR and 2nd harmonic ECR.

Chapter 3

Experimental Setup

3.1 ECH system in VEST

ECH launching system of VEST has been designed to use low field side X-mode injection configuration based on the preliminary experimental result using linear device. As explained in section 1.2, the results from the preliminary experimental showed that low field side injection of microwave with X-mode polarity is most favorable for pre-ionization. Table 3.1 summarizes the parameters of the linear device and VEST such as chamber volume and heating power as well as the estimated maximum electron density in VEST pre-ionization plasma in terms of power density. The heating power of VEST is almost 7 times larger than that of linear device, but heating power density in linear device is almost 78 times larger than that of VEST due to very larger volume of VEST vacuum vessel compared with that of linear device. Note that heating power density is the value of the maximum ECH power divided by the chamber volume. Therefore, the electron density in VEST pre-ionization plasma is estimated to be order of

$10^{16} m^{-3}$ with 6 kW of injected ECH power, which is almost two order smaller than the electron density measured at the linear device. However, if the wave energy is mainly absorbed in main chamber of the VEST, the effective heating volume in VEST will be smaller than total volume of the chamber, and the actual electron density can be higher than the estimated value.

	Linear Device	**VEST**
Chamber Volume [m^3]	7.07×10^{-3}	3.68
Heating Power [kW]	0.9	6
Heating Power Density [kW/ m^3]	127	1.63
Maximum Electron Density [m^{-3}]	$\sim 9 \times 10^{17}$	$> 10^{16}$

Table 3.1 Comparison between the linear device and VEST for estimation of the electron density of VEST pre-ionization plasma

Figure 3.1 shows the installed microwave generator, waveguide and microwave components for low field side injection. The frequency of 2.45GHz and the maximum power of 6kW can be operated with pulse or CW mode. Rectangular waveguide is used to guide the wave in a chosen direction. WR284 and WR340 are installed for propagation of the TE10 mode. For X-mode injection, electric field of microwave must be perpendicular to the toroidal magnetic field. TE10 mode has a linearly polarized electric field perpendicular to the toroidal magnetic field. Cutoff frequency of rectangular waveguide is given by [19]

$$f_c = \frac{1}{2a\sqrt{\mu_0 \varepsilon_0}} \tag{3.1}$$

Where a is width of the waveguide, μ_0 is the permeability in vacuum and ε_0 is the permittivity in vacuum. For the frequency of 2.45GHz, only TE10 mode can propagate in WR284 and WR340 from the equation (3.1). O-mode can be launched using the twisted waveguide which rotate the electric field through 90 degrees.

Microwave components such as directional coupler, rf power meter and 3-stub tuner are installed with waveguide. The directional coupler and rf power meter is utilized for microwave power monitoring during discharge. Forward ECH power and reflected ECH power is attenuated in directional coupler and rf power meter converts the power of microwave into the electrical signals. For effective coupling between the microwave and plasma, impedance matching is set through the reflected microwave power measured with rf power meter and 3-stub tuner.

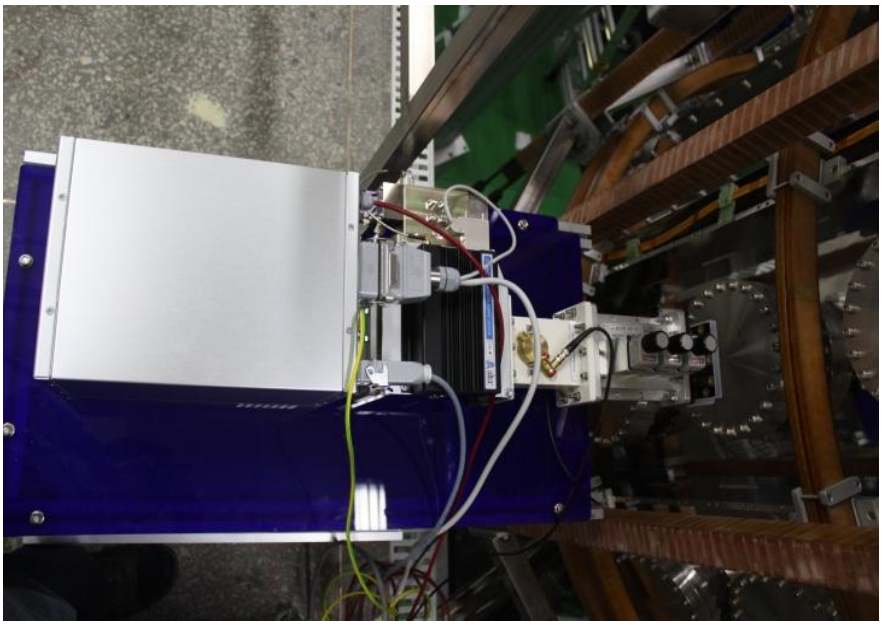

Figure 3.1 Picture of microwave generator, waveguide and microwave components installed in VEST

3.2 Diagnostics

3.2.1 Triple Probe

In this experiment, the triple probe is used mainly to diagnose the time varying plasma during discharges. The triple probe consists of three tips at different potentials. Figure 3.2 shows the schematic diagram of the potential at three tips. The triple probe is combination of floating probe and double probe. The biggest advantage of the triple probe is instantaneous measurement of the electron density and temperature within a short time.

The response time of the triple probe is about lower than 1μsec [20]. Because of the characteristics of direct diagnosis without voltage sweep, the triple probe is useful for many pulsed operation plasmas.

Figure 3.3 shows the schematic diagram of the triple probe circuit. The potential difference and current between each tip is measured using the isolation amplifier AD210AN. The relation of the currents and potentials can be expressed by

$$\begin{aligned} 0 &= SJ_i(V_f) - SJ_e \exp(-\phi V_f) \\ -I &= SJ_i(V_+) - SJ_e \exp(-\phi V_+) \\ I &= SJ_i(V_-) - SJ_e \exp(-\phi V_-) \end{aligned} \tag{3.2}$$

where S is surface area of the probe tips, J_e is the electron saturation current and J_i is the ion saturation current and $\phi \equiv e/kT_e$. If the variation of the ion saturation current is negligible compared with that of the electron current, the ion saturation current is given by

$$J_i(V_f) = J_i(V_+) = J_i(V_-) = J_i \tag{3.3}$$

Then, equation (3.2) and (3.3) yield

$$\frac{1-\exp(-\phi V_{d2})}{1-\exp(-\phi V_{d3})} = \frac{1}{2} \tag{3.4}$$

where $V_{d2} = V_+ - V_f$ and $V_{d3} = V_+ - V_-$. The electron temperature can be obtained from the equation (3.4) by iteration. The elimination of the electron saturation current from the equation (3.2) and equation (3.4) leads to

$$J_i = \frac{I}{S}[\exp(\phi V_{d2}) - 1] \tag{3.5}$$

and ion saturation current is given by [20]

$$J_i = \frac{S'}{S} J_{is} \cong J_{is} = e n_{is} v_{is} = e n_e \exp\left(-\frac{1}{2}\right) \cdot \left(\frac{kT_e}{m_i}\right)^{\frac{1}{2}} \tag{3.6}$$

The equation (3.5) and (3.6) gives the electron density as follows

$$n_e = \left(\frac{(m_i)^{\frac{1}{2}}}{S} I\right) \cdot \frac{\exp\left(\frac{1}{2}\right)}{e(kT_e)^{\frac{1}{2}}[\exp(\phi V_{d2}) - 1]} \tag{3.7}$$

The electron temperature and density is given from the equation (3.4) and (3.7). V_{d2} and I is measured quantity and V_{d3} is a bias voltage that can be controlled. V_{d2} determines the electron temperature and then the electron density can be calculated from I and the electron temperature.

Figure 3.4 is a picture of fabricated triple probe which consist of tungsten wire for probe tips and ceramic tube for electrical insulation. The design requirements are considered relating to assumptions for triple probe theory. It is assumed that interaction effects between probe tips are negligible and probe theory is developed in collisionless sheath. These assumptions can be expressed by $\lambda_{mfp} >> d_s$, $\lambda_{mfp} >> r_p$ and $d_s << s$ where λ_{mfp} is the mean free path of the electrons, d_s is thickness of the sheath and r_p is radius of the probe tip and s is the separation between the probe tips. The assumptions for the mean free path are easily satisfied in VEST operating condition and thickness of the sheath can be estimated by the Debye length. Thus, design requirements for probe tip radius and separation between probe tips are determined by the electron density and temperature of target plasma. Table 3.2 shows the summarized parameters for VEST pre-ionization plasma. The triple probe is fabricated fulfilling the requirements with tip radius of 0.15mm and the separation of 3mm. The length of probe tip is larger than radius of probe tip for cylindrical probe. A bias voltage V_{d3} is chosen to 27V considering the relation between noise level and measured electron temperature. Figure 3.5 shows the electron temperature with respect to bias voltage and measured voltage. As bias voltage decrease, plasma perturbation is decreased but steep slope of the graph in figure 3.5 causes that the electron temperature is sensitive to noise. For the electron temperature of target plasma, bias voltage of 27V is chosen as appropriate value.

Parameters for target plasma	**Value**
Electron density [m^{-3}]	$>10^{16}$
Electron temperature [eV]	<30
Debye length [mm]	<0.04
Radius of probe tip [mm]	0.15
Separation between probe tips [mm]	3
Length of probe tip [mm]	5.5

Table 3.2 Parameters for VEST pre-ionization

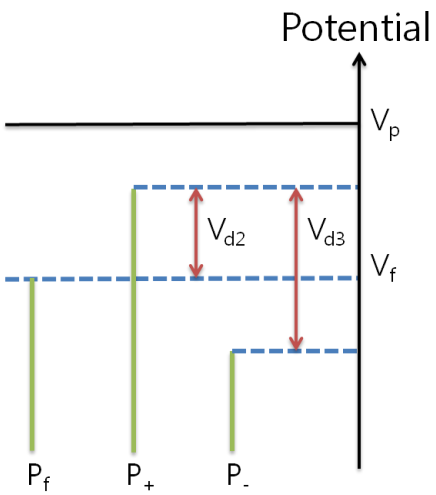

Figure 3.2 Schematic diagram of potential at each tips

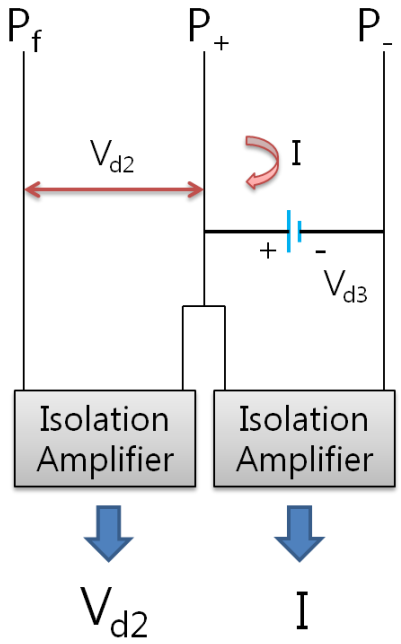

Figure 3.3 Schematic diagram of the triple probe circuit

Figure 3.4 Picture of the fabricated triple probe

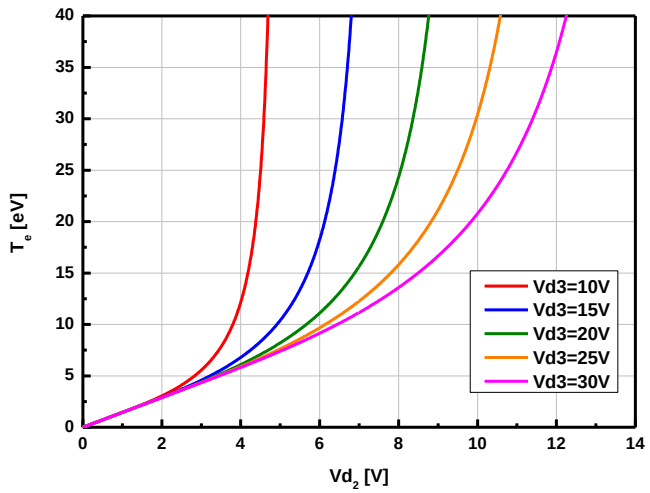

Figure 3.5 Variation of the electron temperature with respect to bias voltage and measured voltage

3.2.2 Comparison with interferometer

To confirm the validity of the triple probe data, 94GHz interferometer [21] installed in VEST is used. Figure 3.6 shows the electron density measured with the triple probe and interferometer. From the radial profile of the electron density measured by the triple probe and line averaged density measured by interferometer, absolute value of the electron density is modified. The electron density measured by the triple probe is similar to modified electron density within the error range. It is shown that the triple probe gives overestimated electron density compared with interferometer data.

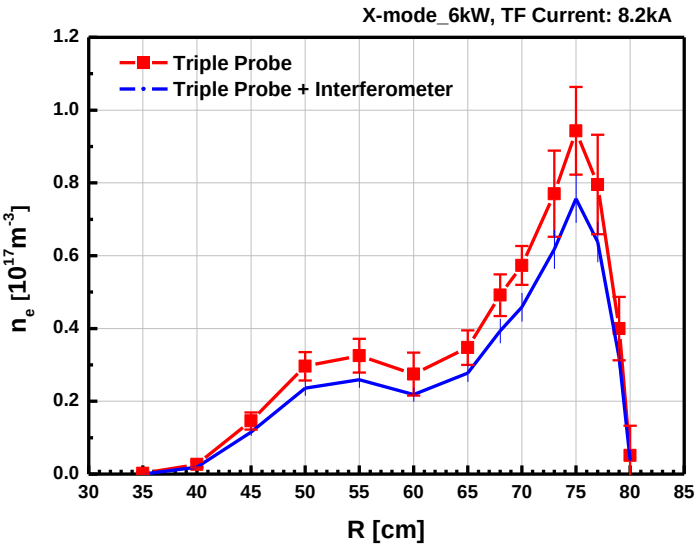

Figure 3.6 The electron density measured with the triple probe and interferometer

Chapter 4

Results

In this chapter, characteristics of ECH plasma in pre-ionization phase with respect to operation parameters such as ECH power, TF strength and wave polarization will be analyzed through the experimental data and inhomogeneous cold plasma model. The theory based on inhomogeneous plasma predicts that the tunneling and mode conversion of X-wave is possible near the R-cutoff layer and upper hybrid resonance (UHR). The results of X-

wave injection are analyzed by Budden model, and then comparison between X-mode and O-mode injection result is discussed.

4.1 The result of X-mode injection

In this experiment radial profiles of the electron density and temperature are measured with triple probe to study the ECH plasma in pure toroidal magnetic field without loop voltage. Experimental conditions are driving frequency of 2.45GHz, operating pressure of 2×10^{-5} Torr and launched wave polarization of X-mode. ECH power and TF current are varied to examine the effect of each parameter on pre-ionization in VEST. Base pressure of VEST is about 1.5×10^{-6} Torr during discharge and working gas is hydrogen. Table 4.1 shows the summarized experimental condition.

Operation Parameters	**Value**
Gas Species	Hydrogen
Base pressure	1.5e-6 Torr
Operating Pressure	2e-5 Torr
TF Current	3.8 / 5.4 / 6.7 / 8.2 kA
ECH Power	2 / 3 / 4 / 6 kW
Driving Frequency	2.45GHz
Wave Polarization	X-mode

Table 4.1 Experimental condition

4.1.1 The effect of ECH power on pre-ionization

To see the ECH power effect on pre-ionization, microwave power is varied from 2kW to 6kW at fixed TF current of 8.2kA. Figure 4.1 shows the radial profile of electron density with respect to the injected ECH power. Error bar in graph means the time variation of the electron density during pre-ionization phase. Two peaks are clearly observed in the fundamental ECR and the UHR with increasing the ECH power. Higher peak is formed near the UHR and lower peak is formed near the fundamental ECR. Radial profile of the electron density is moved to edge as ECH power increase. The UHR is originally identical to the fundamental ECR without the plasma density and gradually separated from the ECR with electron density build-up as shown in relation of the upper hybrid frequency.

$$\omega_{UH} = \sqrt{\omega_{pe}^2 + \omega_{ce}^2} \tag{4.1}$$

When the ECH power is higher than 3kW, the UHR is distinct from the ECR and two peaks appear. As injected ECH power increase, produced higher electron density makes profile move to edge of the chamber satisfying the required density of the UHR and steep density gradient is observed in front of the outer wall.

Figure 4.2 shows the radial profile of the electron temperature with respect to the injected ECH power. The electron temperature profile has a

peak near the fundamental ECR layer, which is positioned at R=45cm, unlike the electron density profile. It is observed that electron temperature peak is shifted from the fundamental ECR layer, which is calculated from the electron cyclotron frequency, to low field side in all data. Shift of resonance layer is caused by the Doppler shift and relativistic effect in wave-particle resonance condition. Wave-particle resonance condition is given by [18]

$$\omega = \frac{n\omega_{ce}}{\gamma} + k_{ll} v_{ll} \tag{4.2}$$

Where $\gamma = 1/\sqrt{1 - v^2/c^2}$. Factor γ gives the relativistic effect and $k_{ll} v_{ll}$ gives the Doppler shift near the resonance layer. n=0 means the Landau damping and n=1 means the fundamental cyclotron damping. In this experiment relativistic effect will be dominant in the wave-particle resonance condition because wave is launched from low field side perpendicular to the toroidal magnetic field. If the relativistic effect is only considered in equation (4.2), real resonance layer where the wave energy is strongly transferred to particles is shifted to low field side region because of $\gamma > 1$.

To investigate the wave power deposition, profile of the electron pressure that means the energy per unit volume is calculated from the radial profile of electron density and temperature. Figure 4.3 shows the radial profile of the electron pressure. When ECH power is higher than 3kW, two peaks are clearly observed in both the UHR and fundamental ECR indicating that X-wave launched from low field side is strongly absorbed in these resonance

layers.

Figure 4.4 is a plot of various resonance and cutoff frequency in case of 6kW injection to investigate the position of the resonance and cutoff. The position of the UHR and R-cutoff is R=78.3cm and R=79.2cm. X-wave launched from low field side first encounters the R-cutoff before reaching the UHR. But the energy of microwave is transferred beyond the R-cutoff layer as shown in figure 4.3. To analyze the tunneling effect, inhomogeneous cold plasma model must be considered. A distance between the UHR and R-cutoff is about 9mm, which is much shorter than a wavelength of 12cm. Maximum electron density of the pre-ionization plasma in VEST is below the L-cutoff density. Therefore, Budden model can be applied for describing the X-wave in the resonance-cutoff pair region.

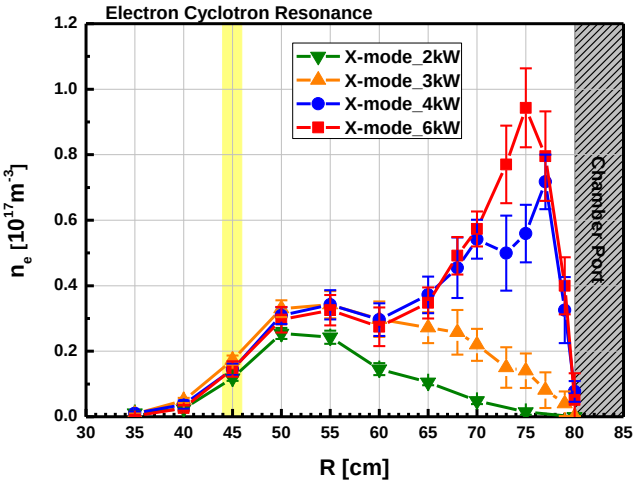

Figure 4.1 Radial profile of the electron density with respect to the ECH power at 2kW/3kW/4kW/6kW

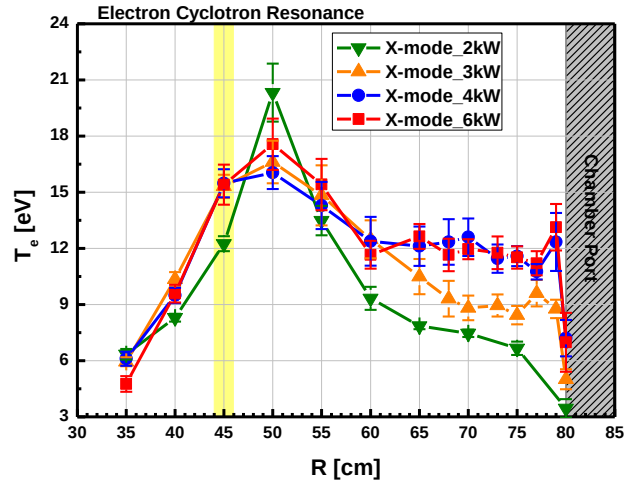

Figure 4.2 Radial profile of the electron temperature with respect to the ECH power at 2kW/3kW/4kW/6kW

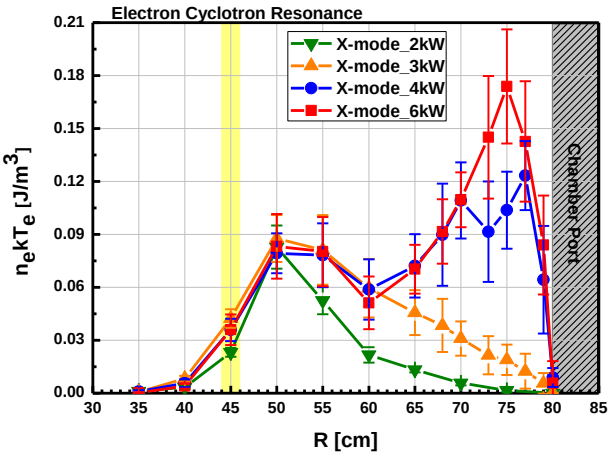

Figure 4.3 Radial profile of the electron pressure with respect to the ECH power at 2kW/3kW/4kW/6kW

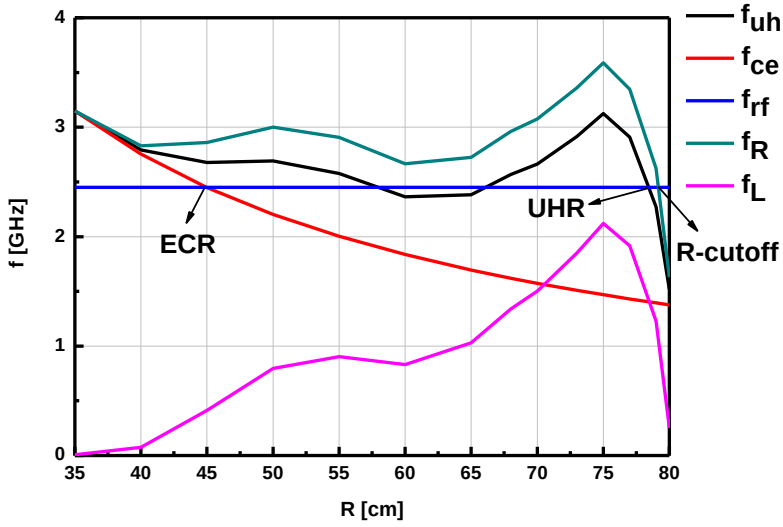

Figure 4.4 Frequency of resonance and cutoff when the ECH power is 6kW

Figure 4.5 shows the time evolution of the electron density measured with triple probe when ECH power of 6kW is injected. Initial breakdown occurs at the fundamental ECR and then electron density peak move towards the outer wall with a separation between the ECR and UHR. Estimation of tunneling and conversion phenomena is possible by Budden analysis. From the radial profile of electron density, a distance between the UHR and R-cutoff that determine the coefficients of the Budden analysis can be calculated.

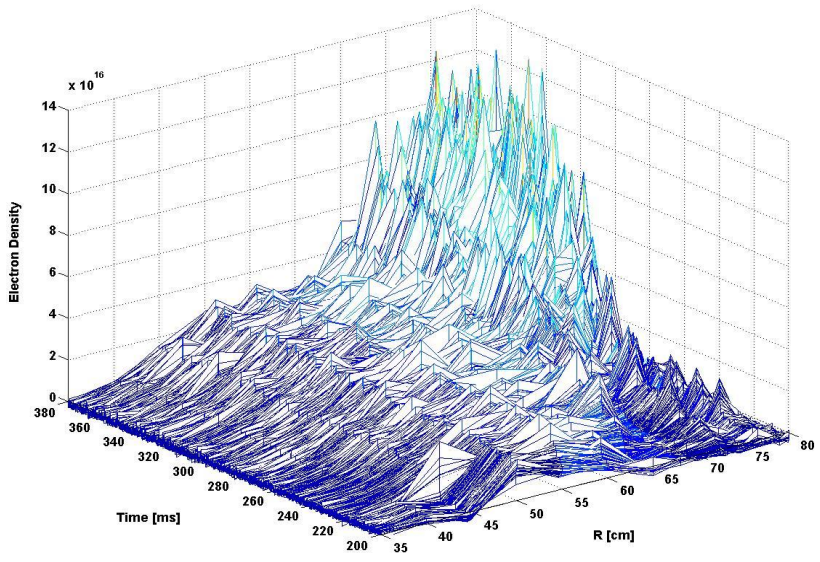

Figure 4.5 Time evolution of the electron density during discharge when ECH power is 6kW

Figure 4.6 shows the time evolution of calculated transmission (T), reflection (R) and conversion (C) coefficients. At the beginning of the breakdown, most X-wave can propagate to resonance layer with the high transmission coefficient. At the ECH power ramp-up phase, plasma starts to expand with increasing the reflection coefficient. Finally the self consistent electron density profile is maintained by X-wave. X-wave is transmitted and reflected as X-wave at the R-cutoff and converted into the EBW at the UHR. The mode conversion coefficient of about 20% is obtained in VEST pre-ionization plasma. Figure 4.7 shows the reflected microwave measured by RF power meter during discharge. The reflection coefficient calculated from experimental data shows good agreement with measured reflected microwave. The tunneling and mode conversion phenomena of X-wave in VEST are well described by Budden analysis.

Experimental data show that wave energy is absorbed in the fundamental ECR and the UHR beyond the cutoff. From the Budden analysis, fraction of reflected wave at cutoff can be lower than half of the incident wave unlike prediction of the homogeneous cold plasma model. The tunneling and mode conversion can occur due to the very steep density gradient in edge region supported by the chamber wall. More detailed discussion is presented in section 4.1.2.

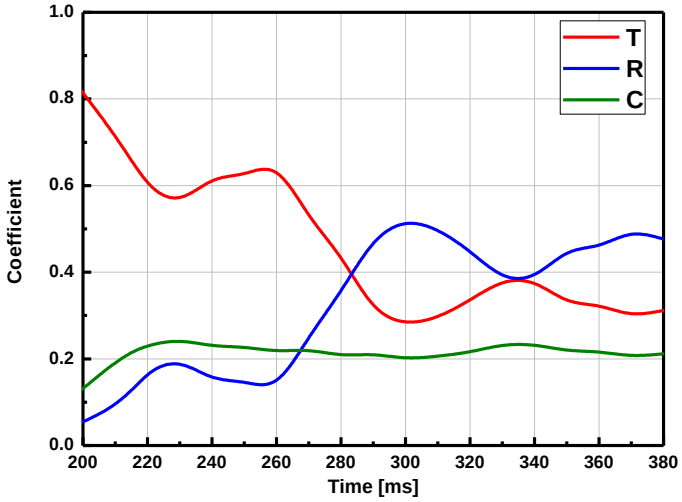

Figure 4.6 Time evolution of calculated transmission, reflection and conversion coefficient

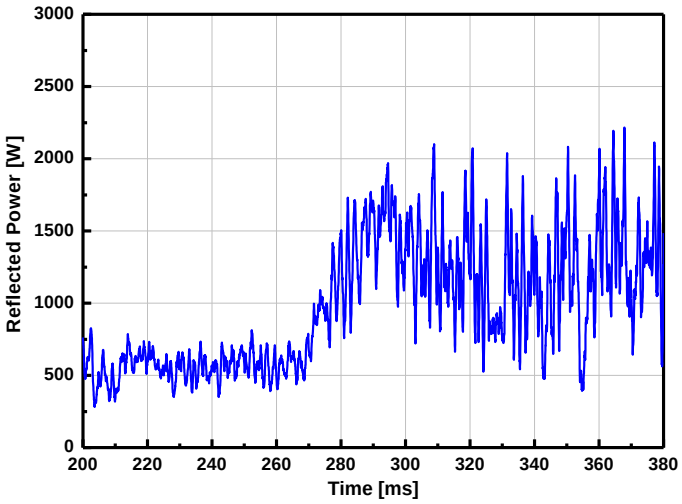

Figure 4.7 Reflected microwave measured by RF power meter

4.1.2 The effect of TF strength on pre-ionization

Because the TF strength affects the position of resonance layer and particle confinement, the TF current is an important operating parameter. To investigate the effect of TF strength on the electron density and temperature profile in pre-ionization phase, the TF current is varied from 3.8kA to 8.2kA at fixed ECH power of 6kW. Figure 4.8 (a)-(d) shows the change of the electron density profile with variation of the TF current. As the TF current decrease, the electron density profile moves to the inboard side along the resonance layer and the plasma density is decreased except the case of the lowest TF current. Table 4.2 shows a calculated transmission, reflection and conversion coefficient of each TF current. As TF current decrease from 8.2kA to 5.4kA, transmission and conversion coefficients are decreased maintaining low plasma density as shown in figure 4.8 (b)-(c). When the TF current is 3.8kA, the transmission and mode conversion coefficient tend to increase again producing the high electron density in the inboard side as shown in figure 4.8 (a).

TF Current	T	R	C
8.2kA	0.2754	0.5251	0.1995
6.7kA, 5.4kA	0.05	0.9	0.05
3.8kA	0.123	0.7691	0.1079

Table 4.2 Transmission, reflection and conversion coefficient for each TF current

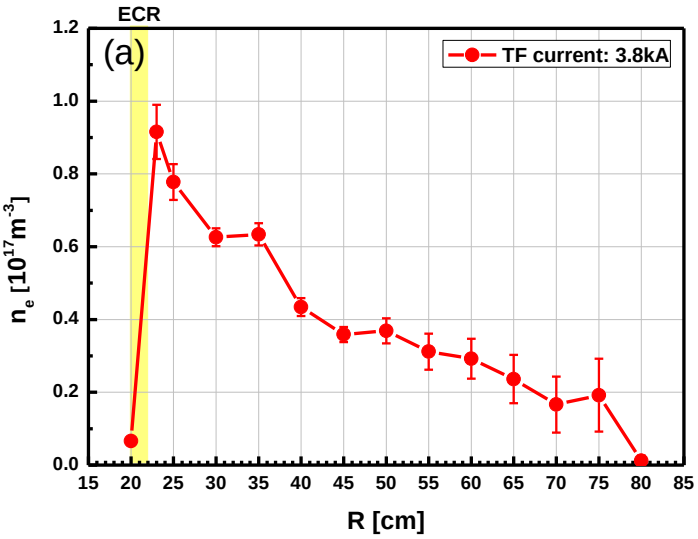
ECR
(a)
TF current: 3.8kA
1.2
1.0
0.8
0.6
0.4
0.2
0.0
n_e [$10^{17}$$m^{-3}$]
15 20 25 30 35 40 45 50 55 60 65 70 75 80 85
R [cm]

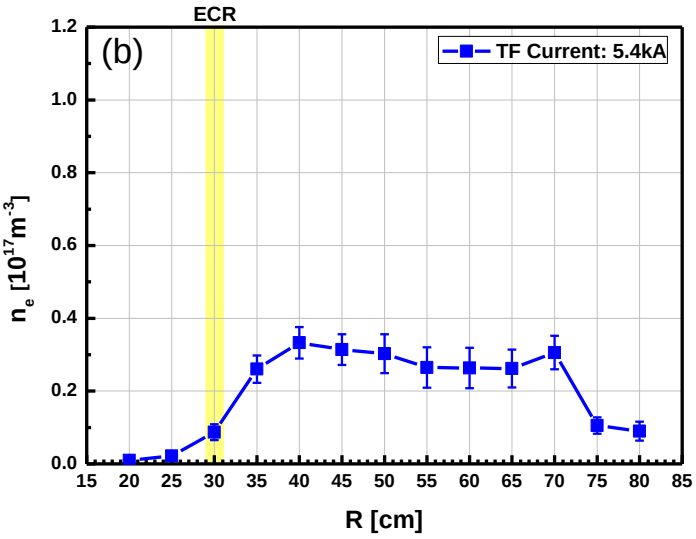
ECR
(b)
TF Current: 5.4kA
1.2
1.0
0.8
0.6
0.4
0.2
0.0
n_e [$10^{17}$$m^{-3}$]
15 20 25 30 35 40 45 50 55 60 65 70 75 80 85
R [cm]

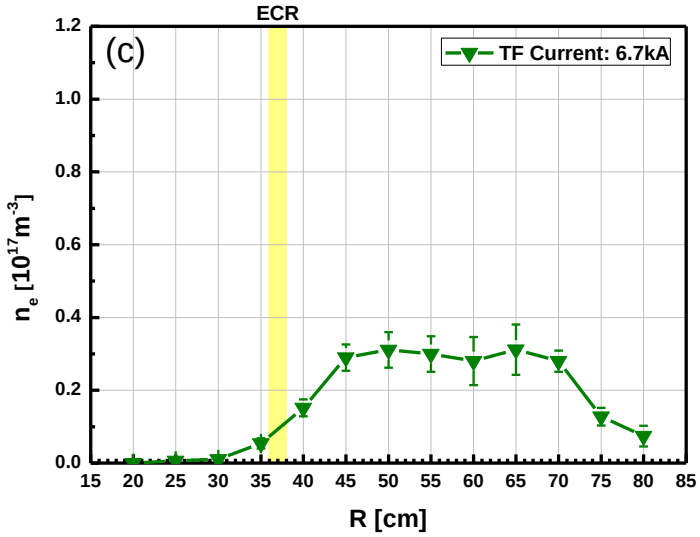

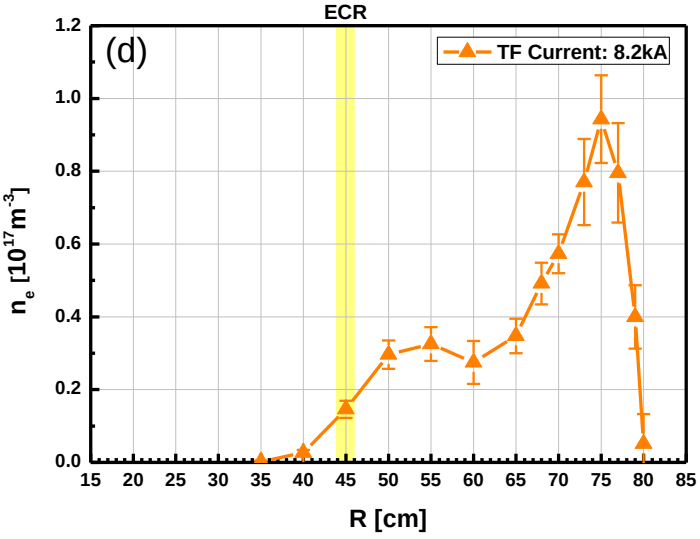

Figure 4.8 The change of the electron density profile with variation of the TF current (a) 3.8kA, (b) 5.4kA, (c) 6.7kA, (d) 8.2kA

This result can be explained by the relation between thickness of the evanescent layer and the plasma parameters. Budden parameter is directly determined by thickness of the evanescent layer as explained in section 2.2.1. A distance between the R-cutoff and UHR can be expressed by the density scale length and magnetic field when the magnetic field scale length is much larger than the density scale length. [22]

$$a = 2L_n k(\sqrt{k^2+1} - k) \tag{4.3}$$

where the factor $k = \omega_{ce} / 2\omega_{pe}$ is evaluated at the R-cutoff. From the above relation, it is shown that density scale length is the dominant factor and magnetic field strength is a second factor in determining the Budden parameter. Steep density gradient in the edge region is maintained by support of the chamber wall when TF current is 8.3kA. A very small density scale length in resonance-cutoff pair region make it possible for X-wave to propagate beyond the evanescent region and to convert into the EBW. As TF current decrease, the resonance layer and the electron density peak move away from the outer chamber wall increasing the density scale length. Despite the advantage of low magnetic field, the increase of the density scale length reduces the fraction of tunneling and mode conversion of X-wave when the TF current is 6.7kA and 5.4kA. When the TF current is 3.8kA, the transmission and conversion coefficient are increased to about half of the TF current of 8.2kA case. But high density plasma comparable to that of 8.2kA is

produced near the CS unlike the result of Budden analysis.

There are two reasons for the different result between experimental data of the lowest TF current and Budden analysis. First, assumption of the Budden model is broken in case of very low TF strength giving the underestimated mode conversion coefficient. As explained in section 2.2.1, Budden model can be applied in resonance-cutoff doublet configuration. But when TF current is very low, resonance layer is positioned in front of the center stack and reflected wave from inner wall of the chamber makes configuration similar to cutoff-resonance-cutoff triplet case explained in section 2.2.2. In this case, application of the Budden model is not practical. The inner wall near the resonance layer plays a role of high density cutoff layer like L-cutoff that reflects incident X-wave back into the resonance layer. Reflected waves into the resonance layer can contribute to the increase of mode conversion efficiency higher than prediction of the Budden model. Secondly, power density absorbed in resonance layer is increased with lower TF current. As TF current decrease, volume of the energy absorption zone is decreased increasing the power density in this region. Therefore, plasma feels that higher power density wave is injected in absorption zone.

4.1.3 Second harmonic heating effect

In section 4.1.2 the electron density profiles of each TF current are discussed. The electron temperature profiles give information of the second harmonic heating effect in the low TF strength experiment. Figure 4.9 shows the change of the electron temperature profile with variation of the TF current. Two temperature peaks are observed near the ECR layers when both the fundamental and 2^{nd} ECR layer exists in the chamber. But X2 mode breakdown without the fundamental ECR layer in the chamber is fail indicating that pre-heated plasma is needed for second harmonic heating. As explained in section 2.3, experimental data shows that second harmonic heating is a FLR effect caused by finite electron temperature. It is observed that heating efficiency at the 2^{nd} harmonic ECR is lower than fundamental heating from the maximum electron temperature near the two resonances.

To analyze the time variation of the electron temperature, forward ECH power and contour plot of temperature are presented. Figure 4.10 shows a contour plot of electron temperature during the discharge and Figure 4.11 shows a forward ECH power measured by RF power meter. Electron temperature peak is located in the fundamental ECR at the beginning of breakdown, and then another peak appears at the ramp-up phase. This result implicate that there is a threshold of power for the second harmonic heating.

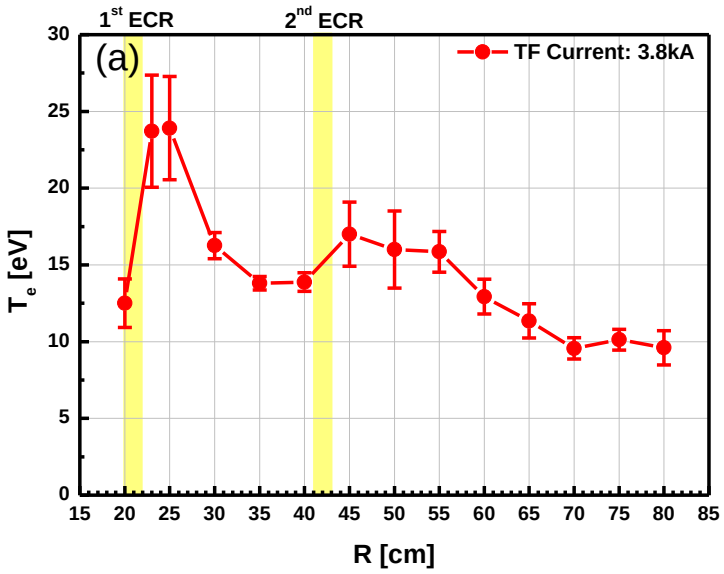
1st ECR
2nd ECR
(a)
TF Current: 3.8kA
T_e [eV]
R [cm]
0
5
10
15
20
25
30
15
20
25
30
35
40
45
50
55
60
65
70
75
80
85

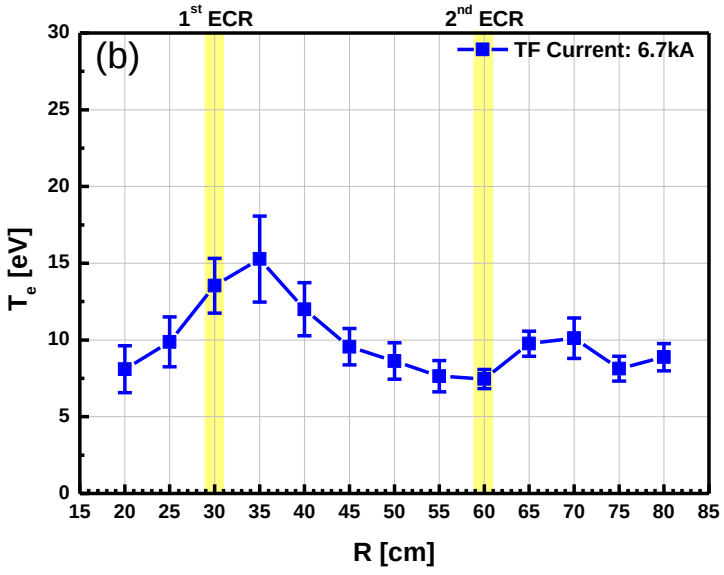
1st ECR
2nd ECR
(b)
TF Current: 6.7kA
T_e [eV]
R [cm]
0
5
10
15
20
25
30
15
20
25
30
35
40
45
50
55
60
65
70
75
80
85

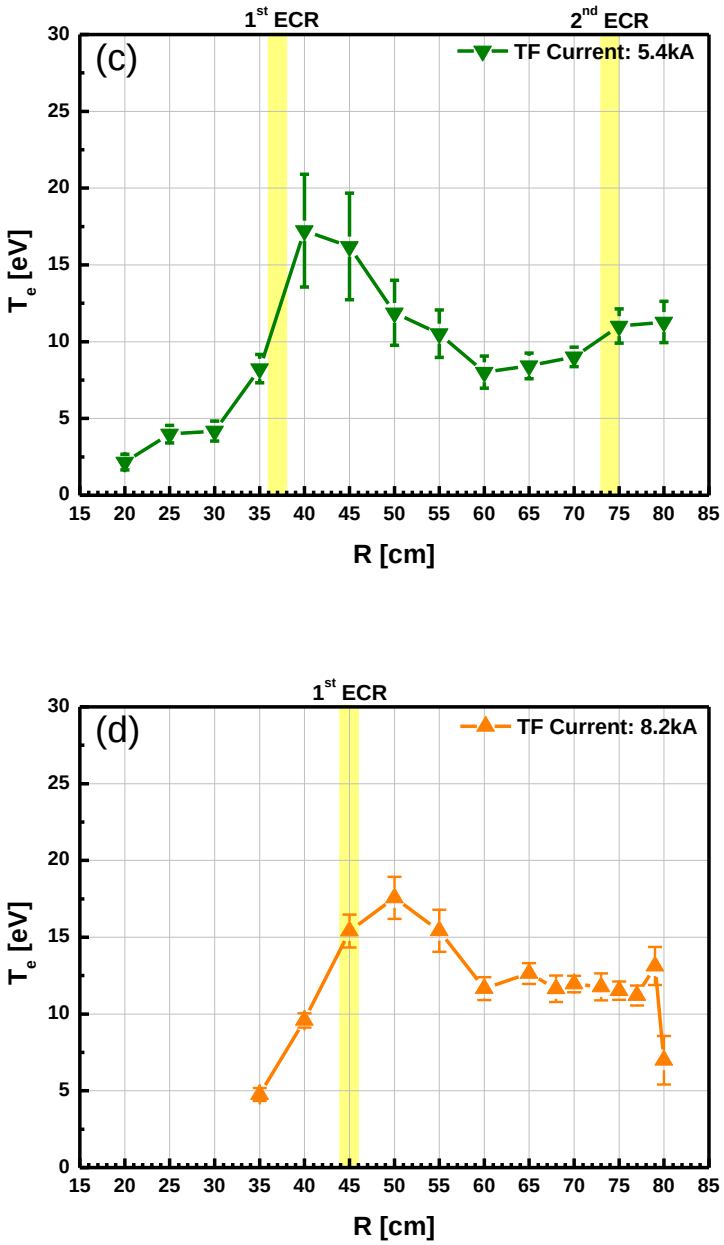

Figure 4.9 The change of the electron temperature profile with variation of the TF current (a) 3.8kA, (b) 5.4kA, (c) 6.7kA, (d) 8.2kA

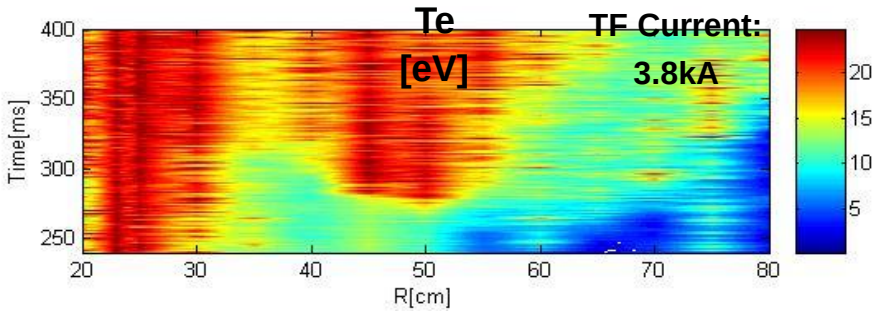

Figure 4.10 Contour plot of the electron temperature during discharge when TF current is 3.8kA

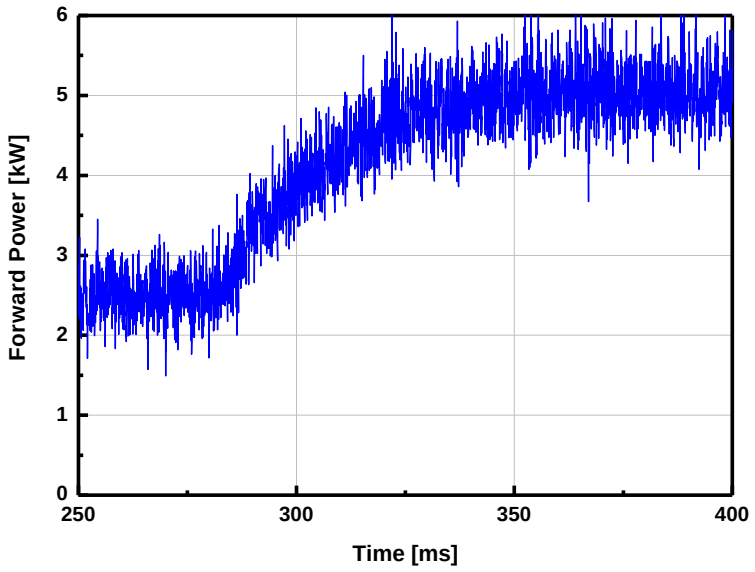

Figure 4.11 Forward ECH power measured by RF power meter

4.2 The result of O-mode injection

To compare the effect of injected wave polarization on pre-ionization plasma, O-mode injection experiment was conducted. Wave polarization can be converted easily using the twisted waveguide in front of the microwave generator. The comparative experiment is conducted with the ECH power of 6kW and TF current of 8.2kA. Other experimental conditions are same as X-mode injection.

Figure 4.12 and Figure 4.13 show the radial profile of the electron density and temperature with respect to the wave polarization. The radial profile data of the O-mode injection is almost same as result of X-mode injection indicating that absorption mechanism for O-mode is similar to X-mode. The electron density of O-mode injection is a little lower that of X-mode injection. Figure 4.14 (a)-(b) show the reflected microwave measured by RF power meter installed in various ports to collect the chosen wave polarization. When X-wave is injected from low field side, most of reflected waves have polarization of X-mode. But when O-wave is injected from low field side, many of the X-mode is detected. From the reflected microwave data, it is shown that the injected O-mode is converted into X-mode in chamber. The reason for mode mixing of O-mode is supposed to multiple reflections between the chamber wall and plasma. With the low ECH power and the consequent low electron temperature so called cold plasma, single pass absorption efficiency of O-mode, which has no resonance in cold plasma, is very low. During the multiple reflections, some fraction of O-mode is

converted into X-mode and then tunneling and mode conversion occurs in the same way as discussed in section 4.1. Therefore, X-mode is more favorable than O-mode for effective pre-ionization with low ECH power.

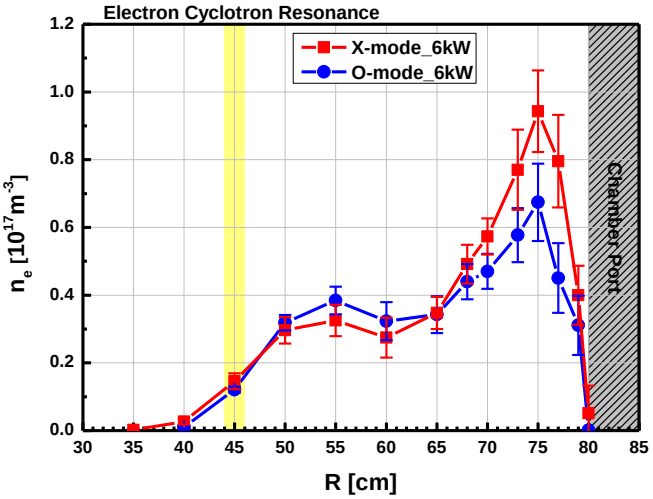

Figure 4.12 Radial profile of electron density with respect to wave polarization

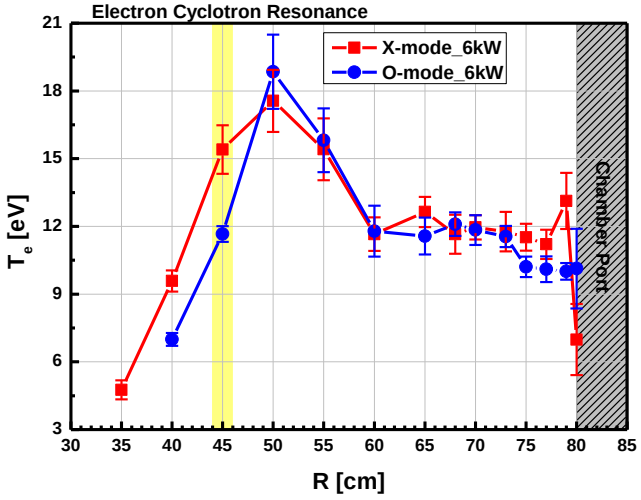

Figure 4.13 Radial profile of electron temperature with respect to wave polarization

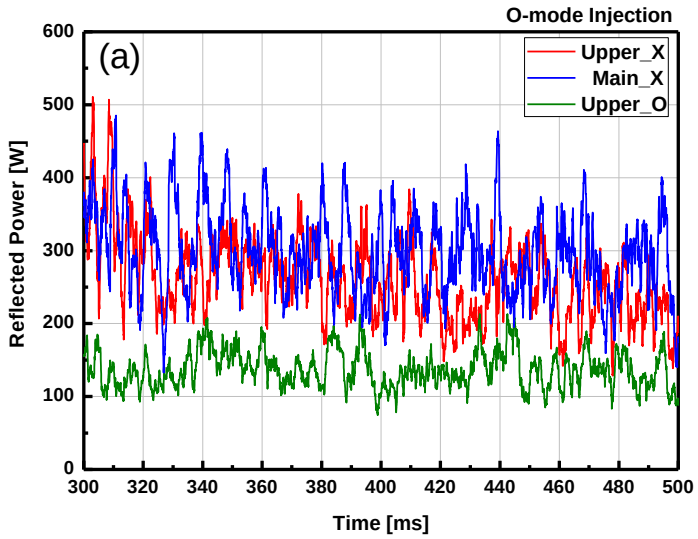

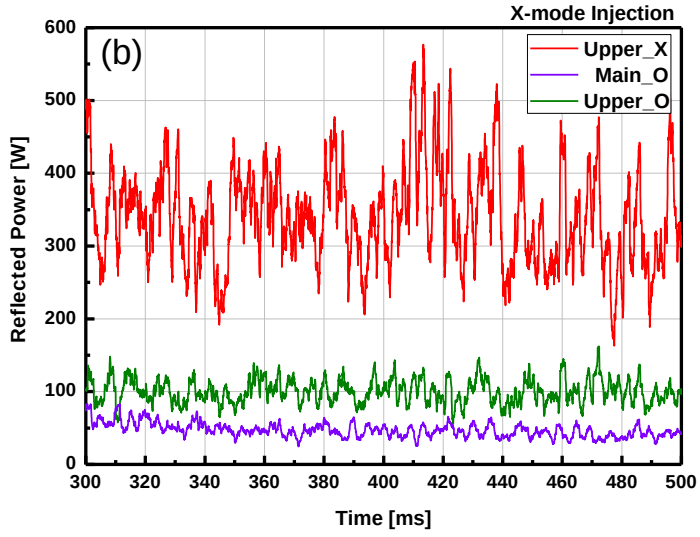

Figure 4.14 Reflected microwave measured with RF power meter
(a) O-mode injection, (b) X-mode injection

Chapter 5

Conclusions

5.1 Summary and conclusions

A study on pre-ionization using ECH is carried out experimentally in VEST to find out the effective pre-ionization condition. The experimental results are analyzed based on inhomogeneous cold plasma model. Especially, Budden analysis is applied in this study to interpret the experimental results of LFS X-mode injection.

The radial profile of electron density and temperature are measured using the triple probe for ECH plasma with toroidal magnetic field only while no loop voltage are provided. The ECH power, TF current and wave polarization are varied to examine the effect of each operation parameter on pre-ionization. It is found that the injected power of X-wave is absorbed in both upper hybrid resonance (UHR) layer and electron cyclotron resonance (ECR) layer. As the injected ECH power increases, the peak of radial electron density profile moves toward outboard side satisfying the required density of the UHR and steep density gradient is observed in front of the outer wall. While only one density peak at ECR layer has been observed with low ECH power, two density peaks are observed in both the ECR and UHR when higher ECH power is provided. As TF current decrease, electron density is

decreased and the resonance layer and the electron density peak move away from the outer chamber wall increasing the density scale length. Despite the advantage of low magnetic field, the increase of the density scale length reduces the fraction of tunneling and mode conversion. With both highest TF current of 8.2 kA and lowest TF current of 3.8 kA, high density plasma is observed. Note that the peak of electron density profile locates near outer wall and inner wall for highest TF current and lowest TF current respectively. The second harmonic heating effect is observed but only when the pre-heated plasma exists and sufficient ECH power is transferred to the plasma. The result of O-mode injection is similar to X-mode injection, which indicates mode mixing. The reflected microwave measured by rf power meter shows that the polarization of O-wave is converted into X-mode in the chamber.

With low field side injection and X-mode polarity, wave propagation beyond the R-cutoff layer has been observed and the energy transfer beyond the cutoff is interpreted as the consequence of tunneling and mode conversion in inhomogeneous plasma. Tunneling and mode conversion phenomena of X-wave in VEST are well described by Budden analysis. The reflection coefficients calculated from the experimental data show a good agreement with measured reflected microwave power. The mode conversion coefficient is calculated to be about 20% in VEST pre-ionization plasma. The density scale length and the magnetic field is dominant factor determining Budden parameter and the consequent coefficients. But the assumption of model must be considered for proper application. When the plasma is produced near the center stack that reflects wave and plays a role of L-cutoff, Budden model

gives underestimated mode conversion efficiency.

In pre-ionization phase, when the plasma parameters such as the electron density and temperature are relatively low, cold plasma resonance must be considered. From the results in this study, the ionization by X-wave and EBW is strongly occurred in the UHR which is described by cold plasma dispersion relation, but injected O-wave has no cold resonance and is hard to be absorbed in UHR layer with low ECH power. Therefore, the LFS X-wave injection with direct X-B mode conversion can be possible as an effective method for pre-ionization in VEST.

In VEST pre-ionization experiment, high density plasma is produced when the peak of density profile is near the inner wall or outer wall with the aid of high X-B mode conversion efficiency. However, in terms of the start-up, these two ways that supported by the inner wall and outer wall have disadvantage of low toroidal magnetic field and high electron density in edge region. For effective pre-ionization, high density plasma must be produced near the center of the chamber without loss of the TF strength. To fulfill these requirements, two schemes can be suggested. First, the magnetic field can be utilized to increase the mode conversion efficiency in center region. During the start-up, high density plasma, which is confined in the magnetic field structure, can make the steep density gradient and L-cutoff layer formed in center region increasing the mode conversion efficiency. Secondly, assistance of the second harmonic heating in the pre-heated plasma by adding another frequency source can be utilized. Although the heating efficiency of second harmonic heating is lower than fundamental heating in pre-ionization phase,

the second harmonic EC wave doesn't encounter cutoff layer before reaching the 2nd harmonic ECR without mode conversion. If the pre-heated plasma exists and sufficient ECH power is injected, the second harmonic heating can be used for central heating with high magnetic field operation.

The characteristic of ECH pre-ionization is investigated with the profile of electron density and temperature to find the effective pre-ionization condition. Also, the effective pre-ionization schemes are suggested based on the experimental results and analysis. This research is expected to contribute to the start-up and EBW study in VEST.

5.2 Future Works

As shown in section 4.2, result of O-mode injection is similar to X-mode injection by mode mixing. But analysis of mode mixing and OXB mode conversion is difficult from present data. More experiment about effect of wave polarization on ECH plasma will be conducted in linear device with the polarizing chamber wall.

In VEST device, 1.5kW of 7.9GHz klystron and 12kW of 2.45GHz magnetrons are under preparation for installation. The role of L-cutoff, which increases the mode conversion efficiency in theory, will be investigated with higher ECH power operation. Also higher cyclotron harmonic effects by the frequency of 7.9GHz will be compared with frequency of 2.45GHz. For more detailed research on ECH pre-ionization, the effect of the field null on radial profile of the electron density and mode conversion will be investigated.

Bibliography

[1] X.K. Yang, Y.P. Zhao, J.G. Li, C.F. Li, Y.G. Shao, Y.Z. Mao, X.M. Gu, D.Z. Xu, J.Y. Ding, D.Y. Xue, X. Deng, J.K. Xie, ‘‘Recent ICRF experiments on HT-7 superconducting tokamak’’, AIP Conf. Proc. 485, 156 (1999).

[2] Battaglia DJ, Bongard MW, Fonck RJ, Redd AJ, Sontag AC, ‘‘Tokamak startup using point-source dc helicity injection’’, Phys Rev Lett, 5;102(22):225003, (2009).

[3] C. Gormezano1, A.C.C. Sips, T.C. Luce, S. Ide, A. Becoulet, X. Litaudon, A. Isayama, J. Hobirk, M.R. Wade, T. Oikawa, R. Prater, A. Zvonkov, B. Lloyd, T. Suzuki, E. Barbato, P. Bonoli, C.K. Phillips, V. Vdovin, E. Joffrin, T. Casper, J. Ferron, D. Mazon, D. Moreau, R. Bundy, C. Kessel, A. Fukuyama, N. Hayashi, F. Imbeaux, M. Murakami, A.R. Polevoi and H.E. St John, ‘‘Chapter 6: Steady state operation’’, Nucl. Fusion 47 S285 (2007).

[4] K. Kajiwara, Y. Ikeda, M. Seki, S. Moriyama, T. Oikawa, T. Fujii and JT-60 Team, ‘‘Electron cyclotron heating assisted startup in JT-60U’’, Nucl. Fusion 45 694 (2005).

[5] Y.S. Bae, J.H. Jeong, S.I. Park, M. Joung, J.H. Kim, S.H. Hahn, S.W. Yoon, H.L. Yang, W.C. Kim, Y.K. Oh, A.C. England, W. Namkung, M.H. Cho, G.L. Jackson, J.S. Bak and the KSTAR team, ‘‘ECH pre-ionization and assisted startup in the fully superconducting KSTAR tokamak using second harmonic’’, Nucl. Fusion 49 022001 (2009).

[6] G.L. Jackson, J.S. deGrassie, C.P. Moeller and R. Prater, ‘‘Second harmonic electron cyclotron pre-ionization in the DIII-D tokamak’’, Nucl. Fusion 47 257 (2007).

[7] S. Alberti, T.P. Goodman, M.A. Henderson, A. Manini, J.-M. Moret, P. Gomez, P. Blanchard, S. Coda, O. Sauter, Y. Peysson, TCV Team, ‘‘Full absorption of third harmonic ECH in TCV tokamak plasmas in the presence of second harmonic ECCD’’, Nucl. Fusion 42 42 (2002).

[8] V.F. Shevchenko, M.R. O’Brien, D. Taylor, A.N. Saveliev and MAST team, ‘‘Electron Bernstein wave assisted plasma current start-up in MAST’’, Nucl. Fusion 50 022004 (2010).

[9] H. Tanaka, T. Maekawa, M. Uchida, T. Yoshinaga, S. Nishi, Y.Kawazu, K.Kurata, T. Takeuchi, ‘‘Non-Solenoidal Formation of Spherical Torus by ECH/ECCD in LATE’’, 22th IAEA Fusion Energy Conf. EX/P6-8, Geneva, Switzerland, (2008).

[10] G. Taylor, P. C. Efthimion, B. Jones, B. P. LeBlanc, J. R. Wilson, J. B. Wilgen, G. L. Bell, T. S. Bigelow, R. Maingi, D. A. Rasmussen, R. W. Harvey, A. P. Smirnov, F. Paoletti, and S. A. Sabbagh, ‘‘Enhanced conversion of thermal electron Bernstein waves to the extraordinary electromagnetic mode on the National Spherical Torus Experiment’’, Phys. Plasmas 10, 1395 (2003).

[11] Syun’ichi Shiraiwa, ‘‘A study of electron Bernstein wave for diagnosis and heating of spherical tokamak plasmas, P.H. thesis, University of Tokyo, (2007).

[12] B. LLOYD, G.L. JACKSON, T.S. TAYLOR, E.A. LAZARUS, T.C. LUCE, R. PRATER, ‘‘Low voltage Ohmic and electron cyclotron heating assisted startup in DIII-D’’, Nucl. Fusion 31 2031 (1991).

[13] Thomas Howard Stix, *Waves in Plasma*. (American Institute of Physics, New York, 1992).

[14] D Gary Swanson, *Plasma Waves, 2nd Edition*. (Institute of Physics Publishing, Bristol and Philadelphia, 2003).

[15] Budden, *The propagation of radio waves*. (Cambridge University Press, Cambridge, 1985).

[16] A. K. Ram, A. Bers, S. D. Schultz, and V. Fuchs, ‘‘Mode conversion of fast Alfven waves at the ion-ion hybrid resonance’’, Phys. Plasmas 3, 1976 (1996).

[17] A. K. Ram and S. D. Schultz, ‘‘Excitation, propagation, and damping of electron Bernstein waves in tokamaks’’, Phys. Plasmas 7, 4084 (2000).

[18] Marco Brambilla, *Kinetic Theory of Plasma Waves: Homogeneous Plasmas*. (Clarendon Press, Oxford, 1998).

[19] Simon Ramo, John R. Whinnery, Theodore Van Duzer, *Fields and Waves in Communication Electronics, 3rd edition*. (John Wiley & Sons, 1994).

[20] SinLi Chen and T. Sekiguchi, ‘‘Instantaneous DirectDisplay System of Plasma Parameters by Means of Triple Probe’’, J. Appl. Phys. 36, 2363 (1965).

[21] Da-Hye Choi, ‘‘Development of interferometer system for versatile experiment spherical torus (VEST)’’, M.S. thesis, Seoul National University (2007).

[22] G J Kramer, R Nazikian and E Valeo, ‘‘Effects of two-dimensional and finite density fluctuations on O-X correlation reflectometry’’, Plasma Phys. Control. Fusion 44 L11 (2002).

국 문 초 록

전이온화는 효과적인 플라즈마 시동을 위해 요구되는 루프 전압과 자속 소비량을 줄이기 위해 미리 플라즈마를 형성하는 과정을 뜻한다. ECH는 대부분의 토카막 장치에서 전이온화 방법으로 많이 쓰이고 있다. 그러나 낮은 자기장에서 높은 밀도로 운전되는 구형 토러스에서는 컷 오프 밀도가 낮기 때문에 대안으로써 EBW를 이용하는 연구가 진행 중이다. 전자 밀도 및 온도의 분포가 전이온화에 미치는 영향에 대한 연구는 기존에 많이 이루어지지 않았다. 본 논문에서는 전자 밀도 및 온도 분포를 측정하여 VEST에서의 ECH를 이용한 전이온화에 대한 연구가 수행되었다.

X-wave의 터널효과와 모드변환을 분석하기 위해서 두 가지 비균일 저온 플라즈마 모델이 소개되었다. 특히 Budden 모델을 적용하여 실험결과를 해석했다.

VEST의 ECH 시스템은 선행 연구 결과의 결과를 기반으로 하여 낮은 자기장 쪽에서부터 X-mode로 입사되도록 설계되었다. 2.45GHz, 최대파워 6kW 입사가 가능한 마그네트론이 설치 되었다. 시간에 따라 빠르게 변하는 플라즈마를 진단하기 위해 트리플 프로브가 제작되었다. 트리플 프로브의 설계 요건들은 선행 연구로부터 예측된 VEST 전이온화 플라즈마의 밀도와 온도에 적합하도록 결정되었다. 트리플 프로브 측정결과의 타당성 검토를

위해서 간섭계와 비교되었다.

루프 전압이 공급되지 않는 토로이달 자기장내에서 만들어진 ECH 플라즈마의 전자 밀도와 온도의 반경분포는 트리플 프로브를 통해 측정되었다. ECH 파워, 토로이달 코일의 전류, 파동의 편광을 변화시키면서 이러한 운전조건들이 전이온화에 미치는 영향 및 최적의 전이온화 조건이 조사되었다. 입사하는 ECH 파워가 증가하였을 때, ECR과 UHR 사이의 거리가 멀어지면서 두 밀도 피크가 측정되었고, 바깥쪽 벽 근처에서 높은 기울기의 밀도 분포가 측정되었다. TF 세기가 감소하면, 전자 밀도의 분포가 공명영역의 위치와 함께 챔버 안쪽으로 이동하게 되고, 최대 밀도 값이 약 30% 정도로 감소하게 된다. 그러나 TF 세기가 더 낮아져 플라즈마가 안쪽 벽 근처에서 형성되는 경우 높은 TF 세기의 경우 만들어지는 플라즈마와 비슷한 밀도가 측정되었다. 제2조파(second harmonic)에 의한 가열효과는 미리 가열된 플라즈마가 존재하고 충분한 ECH 파워가 입사되었을 때만 관측되었다. O-모드 입사 실험 결과는 X-모드 입사 실험 결과와 매우 유사하지만 전자 밀도가 약간 작게 측정되었다. 파워미터로 측정된 반사파 실험 자료를 통해 입사된 O-mode의 경우 챔버안에서 상당 비율이 X-mode로 모드변환 된다는 것을 알 수 있다.

VEST에서 X-모드의 터널효과와 모드변환 현상이 Budden 분석에 의해서 잘 기술되었다. 플라즈마 방전 중에 실험 자료로부터 계산된 반사율 계수와 파워미터로 측정된 반사파가 잘 일치하는

경향을 보인다. VEST 전이온화 플라즈마에서 모드 변환율은 약 20%까지 계산되었다. VEST 전이온화에 번스타인파가 이용 될 수 있음을 확인하였다. 번스타인 파를 전이온화에 활용하기 위해서 밀도 변화율, 자기장의 세기, 챔버 벽이 터널효과와 모드변환에 미치는 효과가 논의 되었다.

VEST 전이온화 실험에서, 전자 밀도 분포의 최대값이 안쪽벽이나 바깥쪽 가까이에 형성될 때 높은 모드 변환율과 함계 높은 밀도의 플라즈마가 형성되었다. 하지만 높은 TF 세기로 운전하면서 중심부 플라즈마가 높은 것이 플라즈마 시동에 유리하다. 효과적인 전이온화를 위해서 두가지 방법이 제시될 수 있다. 첫번째는 플라즈마 시동 중에 자기장 구조를 활용하여 챔버 가운데 영역에서 모드 변환율을 증가 시키는 방법이다. 플라즈마 시동 중에 자기장 구조에 의해 갇힌 고밀도의 플라즈마는 중심부에 급격한 밀도 변화와 L-cutoff을 만들면서 모드 변환율을 증가시킬 수 있다. 두번째는 ECH로 미리 가열되어 있는 플라즈마에 더 높은 주파수의 마이크로파를 추가 입사해 제2조파 가열을 활용하는 방법이다. 비록 제2조파 가열은 주공명가열에 비해 효율이 낮지만 모드변환없이도 컷오프 영역을 지나지 않고 공명영역에 도달가능한 장점이 있다. 제2조파 가열이 높은 토로이달 자기장 운전에서 중심부 가열을 위해 이용될 수 있다.

최적의 전이온화 조건을 찾기 위해서 ECH 전이온화의 특성들이 전자 밀도 및 온도의 분포와 함께 조사되었다. 또한 실험 결과와 분석을 바탕으로 효과적인 전이온화 방법들이 제시되었다.

본 연구는 VEST에서의 플라즈마 시동 및 전자 번스타인파 연구에 공헌 할 수 있을 것으로 기대된다.

주요어: 전이온화, 구형 토러스, 전자 사이클로트론 가열, VEST, Budden 모델, 터널효과, 모드변환, 전자 번스타인파, 전자 사이클로트론 공명,

학 번: 2011-21112